Materials Advances

ROYAL SOCIETY OF CHEMISTRY

PAPER

View Article Online
View Journal | View Issue

Cite this: *Mater. Adv.*, 2022, 3, 6062

Engineering bistetrazoles: (*E*)-5,5′-(ethene-1,2-diyl)bis(1*H*-tetrazol-1-ol) as a new planar high-energy-density material†

Jatinder Singh, [a] Richard J. Staples [b] and Jean'ne M. Shreeve *[a]

Energetic properties of bistetrazole derivatives are improved by the step-by-step introduction of functionalities which improve heat of formation, density, and oxygen content. The incorporation of unsaturation between bis(1*H*-tetrazol-5-yl) and bis(1*H*-tetrazol-1-ol) derivatives leads to planarity which enhances the density of the final product. In this manuscript, we have synthesized compounds 1,2-di(1*H*-tetrazol-5-yl)ethane (**4**), (*E*)-1,2-di(1*H*-tetrazol-5-yl)ethene (**5**), and (*E*)-5,5′-(ethene-1,2-diyl)bis(1*H*-tetrazol-1-ol), (**6**) using readily available starting materials. Their corresponding dihydroxylammonium salts **7**, **8** and **9** are obtained by reacting two equivalents of hydroxylamine (50% in water). New compounds are analyzed using IR, EA, DSC and multinuclear NMR spectroscopy (^{1}H, ^{13}C and ^{15}N). The solid-state structures of compounds **6**, **7**, **8** and **9** are confirmed by single-crystal X-ray diffraction. The energetic performances are calculated using the EXPLO5 (v6.06.02) code and the sensitivities towards external stimuli such as friction and impact are determined according to BAM standard. Compound **6** {(*E*)-5,5′-(ethene-1,2-diyl)bis(1*H*-tetrazol-1-ol)} exhibits a surprisingly high density of 1.91 g cm^{-3} at 100 K (1.86 g cm^{-3} at 298 K). Its detonation velocity (9017 m s^{-1}) is considerably superior to those of RDX (8795 m s^{-1}), which suggests it is a competitive high-energy-density material.

Received 10th June 2022,
Accepted 23rd June 2022

DOI: 10.1039/d2ma00664b

rsc.li/materials-advances

Introduction

Exploration of new energetic derivatives based on the tetrazole ring continues as a key method in developing environmentally friendly materials.[1–3] The tetrazole ring allows facile attachment of a variety of groups to the carbon atom at the five position and substitution on nitrogen at the N1 and N3 positions.[4–8] Over the past decades, many linked or bridged tetrazole derivatives have been developed through the rational combination of tetrazole and substituents such as N═N–, –NH–, –C(O)–, –C–C–, and azole rings.[9–15] The physicochemical properties of linked-tetrazole derivatives can be easily altered by modifying the linking group.[16] For example, pyrazole-linked bis-tetrazoles exhibit better thermal stabilities and insensitivities compared to azo-linked bis-tetrazoles; however, the detonation properties of the latter are found to be far superior.[17] At present, only a few examples of linked-tetrazole derivatives are known to display a balance between safety and energy.[18] Therefore, it is of considerable value to expand the number of these for the construction of high energetic tetrazoles.

The use of tetrazole-based compounds rather than nitro or nitroamino compounds RDX (1,3,5-trinitro-1,3,5-triazinane) and HMX (1,3,5,7-tetranitro-1,3,5,7-tetrazocane) has the advantage of high personal and ecological safety.[19–22] RDX is a potential carcinogen known to be toxic to humans and organisms in the soil. However, the lack of oxygen content in tetrazole derivatives limits their detonation performance and practical applicability in comparison to nitro- or nitroamino-based compounds.[23–27] Replacing the tetrazole ring with 1*H*-tetrazol-1-ol is known to enhance the density, oxygen balance, thermal stability, insensitivity, and detonation power.[28] Notable examples include, 5,5′-bistetrazole-1,1′-diol (1,1-BTO) and dihydroxylammonium 5,5′-bistetrazole-1,1′-diolate (TKX-50) as high-performing high-energy-density materials (HEDMs) (Fig. 1(a)).[29–31]

The introduction of planarity through conjugation is an important strategy for realizing high-performance materials.[32] Planarity in a molecule facilitates efficient packing and maximizes weak non-covalent interactions (π-stacking, anion-π, cation/π, H-bonding, *etc.*), which play vital roles in improving density and thermal stability.[33] In addition, planar stacked

[a] *Department of Chemistry, University of Idaho, Moscow, Idaho, 83844-2343, USA. E-mail: jshreeve@uidaho.edu*
[b] *Department of Chemistry, Michigan State University, East Lansing, Michigan, 48824, USA*

† Electronic supplementary information (ESI) available: Isodesmic reactions, synthesis of compounds **3–9**, DSC analysis, ^{1}H, ^{13}C and ^{14}N NMR data, X-ray crystal structure parameters of **6**, **7**, **8** and **9**. CCDC 2160643–2160646. For ESI and crystallographic data in CIF or other electronic format see DOI: https://doi.org/10.1039/d2ma00664b

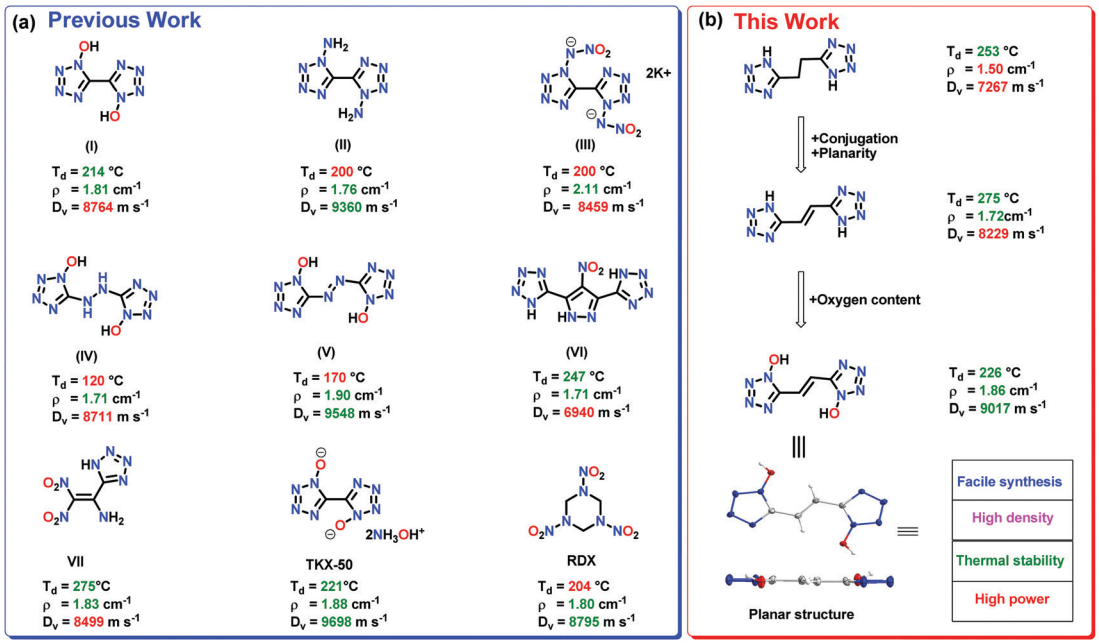

Fig. 1 (a) Representative energetic compounds reported in literature (decomposition temperature $\leq$ 204 °C, density below 1.70 g cm^{-1} and detonation velocities below RDX are given in red, whereas desirable properties are given in green) (b) compounds reported in this study.

layers absorb mechanical energy, which helps in reducing sensitivity toward external stimuli.[34] Attempts to design conjugated planar HEDMs have been made by many researchers. For example, fused tetrazolo 1,2,4,5-tetrazine N-oxides, 4-amino-3,7-dinitro-[1,2,4]-triazolo[5,1-*c*][1,2,4]triazine, and nitroamino-functionalized 1,2,4-triazolo[4,3-*b*][1,2,4,5]tetrazine are planar conjugated structures reported as high-performance materials.[35–37] Recently it was demonstrated that tetrazole or triazole ring substituted FOX-7-like molecules exhibit good thermal stability and improved sensitivity due to the planar conjugated structures.[38–40] Inspired by the good performance of conjugated planar energetic compounds, we speculated that the introduction of a planar conjugated ethene link between tetrazole rings would improve the density, heat of formation and insensitivity.

Now we have synthesized ethane and ethene linked bistetrazole derivatives: 1,2-di(1*H*-tetrazol-5-yl)ethane (**4**), (*E*)-1,2-di(1*H*-tetrazol-5-yl)ethene (**5**), and the ethene-linked bis(1*H*-tetrazol-1-ol) derivative, (*E*)-5,5′-(ethene-1,2-diyl)bis(1*H*-tetrazol-1-ol), (**6**) using readily available starting materials. Dihydroxylammonium salts **7**, **8** and **9** are obtained by reacting two equivalents of hydroxylamine (50% in water) with compounds **4**, **5** and **6**. Compound **6** exhibits the highest density and detonation properties.

Results and discussion

The reaction of succinonitrile (**1**) with sodium azide in the presence of zinc chloride resulted in the formation of 1,2-di(1*H*-tetrazol-5-yl)ethane (**4**), as a white solid in 86% yield (Scheme 1a). Similarly, the reaction of fumaronitrile (**2**) with sodium azide in the presence of zinc chloride gave (*E*)-1,2-di(1*H*-tetrazol-5-yl)ethene (**5**), as a yellow solid in 79% yield (Scheme 1b). (*E*)-5,5′-(ethene-1,2-diyl)bis(1*H*-tetrazol-1-ol) (**6**) was obtained in four steps from **2**. The reaction of **2** with hydroxylamine (50% in water) resulted in the formation of the diamidooxime derivative, which when reacted with $NaNO_2$/HCl gave the dichlorooxime derivative (Scheme 1c). The latter with sodium azide (NaN_3) formed compound **3** which when treated with gaseous HCl in diethyl ether resulted in **6** as an off-white powder. The reactions of **4**, **5** or **6** with two equivalents of hydroxylamine (50% in water) in acetonitrile resulted in the formation of their corresponding energetic hydroxylammonium salt **7**, **8** or **9** (Scheme 1a–c).

All compounds are characterized by NMR (^{1}H and ^{13}C), and infrared (IR) spectroscopy as well as elemental analysis. In the ^{1}H NMR spectrum of compound **6**, the ethene group protons are shifted upfield (7.62 ppm) relative to compound **5** (7.67 ppm) (ESI†). In the ^{13}C{^{1}H} NMR spectrum, signals corresponding to the ethene group carbon atoms in **6** are observed at 116.8 ppm and the tetrazole at 144.0 ppm (ESI†). The ^{15}N NMR spectra of **6** and **9** are given in Fig. 2. In the spectrum of **6**, four signals are seen for the nitrogen atoms of the tetrazole ring at δ = −115.9, −54.2, −17.7 and −1.2, while nitrogen atoms corresponding to compound **9** are seen at δ = −85.1, −57.9, −17.1 and −11.8. The nitrogen atoms of the hydroxylamine cations in **9** are observed at δ = −296.9.

The structures of **6**, **7**, **8** and **9** were further confirmed by single-crystal X-ray diffraction (SC-XRD). Crystals suitable for SC-XRD analysis were obtained through the slow evaporation of a saturated solution in a methanol/water or ethanol/water mixture at room temperature. Crystal structures are given in Fig. 3–6. Crystallographic data and data collection parameters, bond lengths, and bond angles are given in the ESI.† Compound **6** crystallizes in the tetragonal space group $I4_1cd$ with

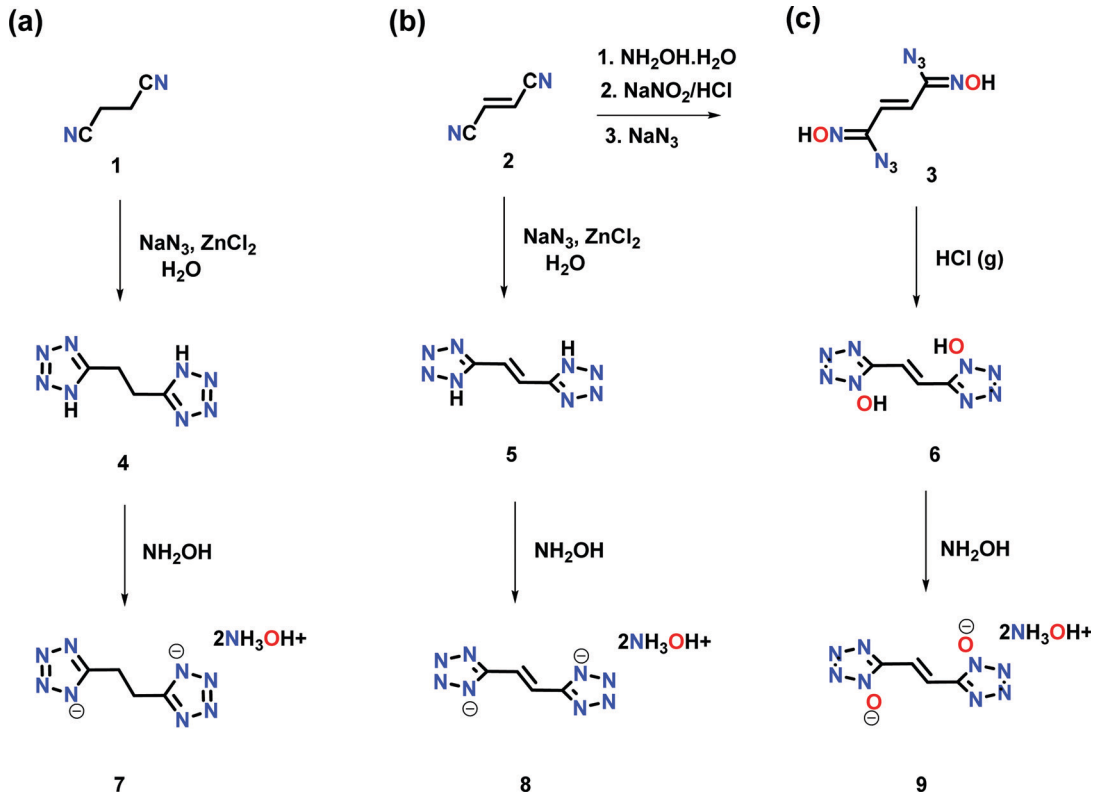

Scheme 1 (a) Synthesis of the ethane-linked bistetrazole derivative **4** and its dihydroxylammonium salt **7**. (b) Formation of the ethene-linked bistetrazole derivative **5** and its dihydroxylammonium salt **8**. (c) Synthesis of the ethene-linked bis(1*H*-tetrazol-1-ol) derivative **6** and its dihydroxylammonium salt **9**.

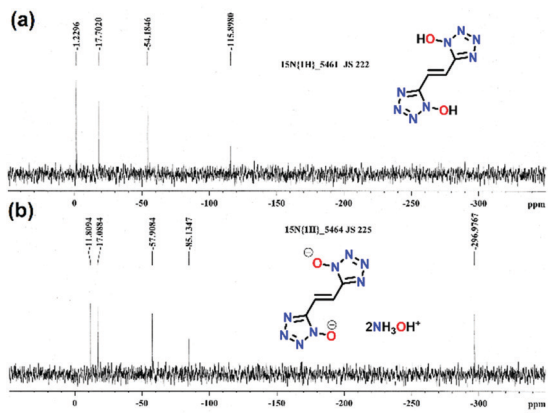

Fig. 2 ^{15}N NMR spectra of (a) **6**, (b) **9**.

eight chemical formula units per unit cell (Fig. (3a)). The calculated crystal density for compound **6** is 1.905 g cm^{-3} at 100 K. Interestingly, the 1*H*-tetrazol-1-ol rings and the ethene bridge are nearly coplanar. In the crystal packing of **6**, strong intermolecular hydrogen bonds and π–π stacking interactions are observed, which make a positive contribution to its density (Fig. 3b and c). The length of the hydrogen bond (O–H···N) is 1.927 Å and the distances of the π–π interactions between the stacked rings range from 3.038 to 3.203 Å.

Compound **7** crystallizes in the orthorhombic space group *Ima*2 with four chemical formula units per unit cell (Fig. (4)). The calculated crystal density for compound **7** is 1.506 g cm^{-3} at 100 K. In the crystal packing of **7**, intermolecular interactions are between the hydroxylamine cations and the bistetrazole anion. The two tetrazole rings are perpendicular to each other. The compound is nonplanar which reduces its crystal density significantly.

Compound **8** crystallizes in the triclinic space group $P\bar{1}$ with one chemical formula unit per unit cell (Fig. (5)). The calculated crystal density for compound **8** is 1.585 g cm^{-3} at 100 K. Relative to compound **7**, compound **8** exhibits higher density due to the planar bistetrazole anions.

All atoms of the ethene-linked bistetrazole rings are coplanar. In addition, intermolecular hydrogen bonding and π–π stacking interactions are observed, which also make a positive contribution to the density. The distance of π–π interactions between the stacked rings is 3.195 Å.

Compound **9** crystallizes in monoclinic space group $P2_1/c$ with four chemical formula units per unit cell (Fig. (6)). The calculated crystal density for compound **9** is 1.668 g cm^{-3} at 100 K. In the crystal packing of **9**, intermolecular interactions are observed between the hydroxylammonium cations and the bis(1*H*-tetrazol-1-olate) anion.

Since crystal packing strongly influences physical properties of energetic compounds, two-dimensional (2D) fingerprints and the associated Hirshfeld surfaces[41,42] are employed by using Crystalexplorer17.5 to understand structure–properties and intermolecular interactions in **6** (Fig. 7a and b). Red and

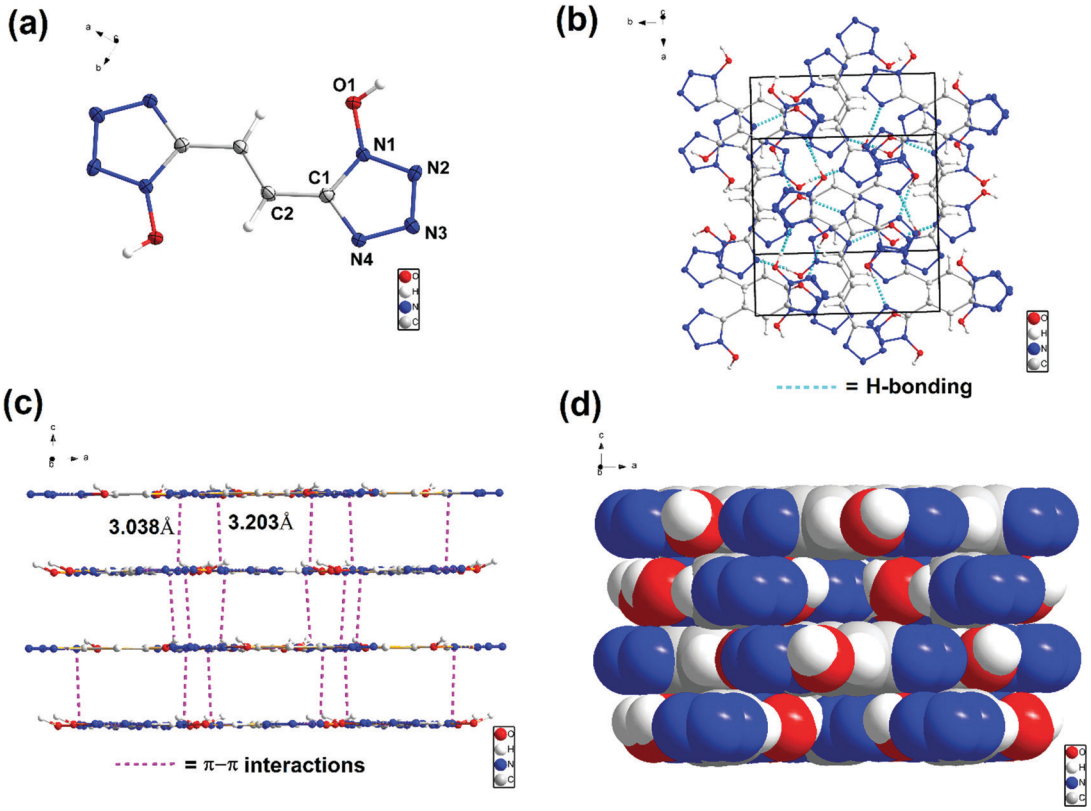

Fig. 3 (a) Thermal ellipsoid (50%) plot and tagging scheme for **6**. (b–d) Packing diagrams of **6**.

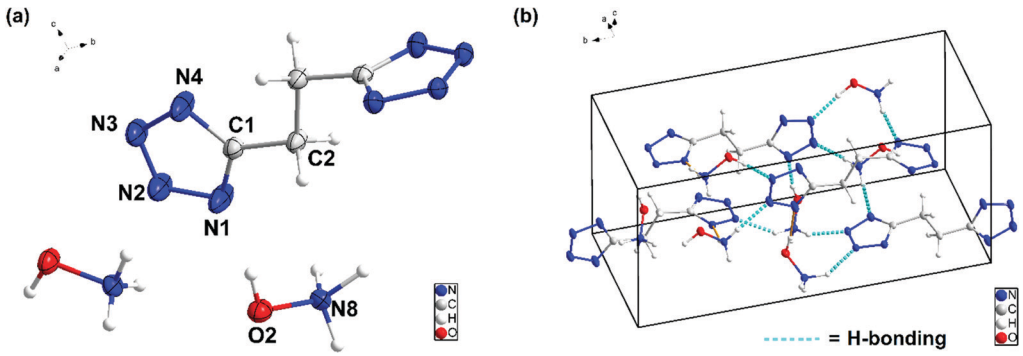

Fig. 4 (a) Thermal ellipsoid (50%) plot and tagging scheme for **7**. (b) Packing diagram of **7**.

blue dots on the Hirshfeld surface represent high and low close contacts, respectively. Strong stabilizing intermolecular (N···H) interactions are observed which contribute to high density and good thermal stability. In addition, high percentages (22.9%) of N···N, and N···C interactions are observed which denote π–π stacking between the molecules. This is also supported by non-covalent interaction (NCI) plots of gradient isosurfaces for **6** (Fig. c). The green surface is seen clearly in Fig. 7c due to the presence of π–π interactions.[43–45] The combination of N···H and π–π interactions leads to the good molecular stability of compound **6**.

Additionally, planar molecules with layered packing and π–π stacking interactions tend to exhibit reduced sensitivity by converting mechanical energy into electrostatic attraction between layers. Specifically, parallel planar-layered packing of molecules can effectively reduce the friction sensitivity (FS). As shown in Fig. 8a and b, FS of compound **6** is significantly larger in comparison to (*E*)-5,5′-(diazene-1,2-diyl)bis(1*H*-tetrazol-1-ol) (V). In comparison to V, the stabilizing interactions in compound **6** also ensure the safe compression of the molecule during impact. The IS and FS of compound **6** is also found to be superior to 5,5′-(hydrazine-1,2-diyl)bis(1*H*-tetrazol-1-ol) (IV) (Table 1).

The thermal behavior of compounds **4–9** was explored using differential scanning calorimetry (DSC) at a heating rate of

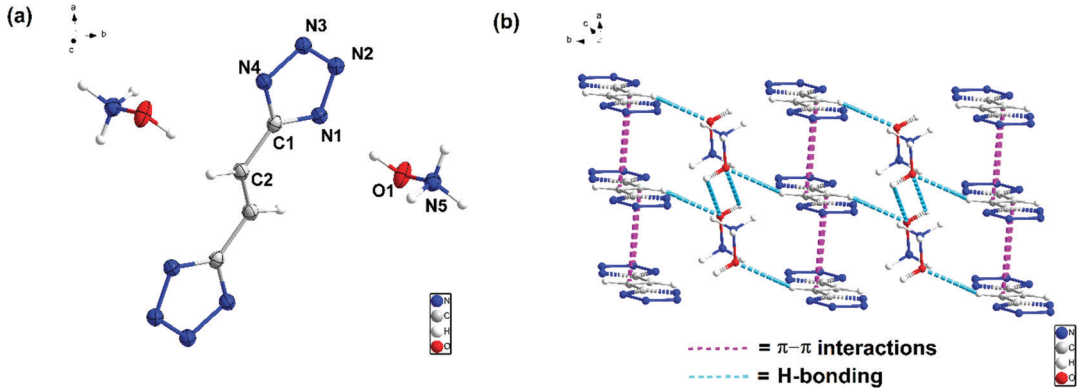

Fig. 5 (a) Thermal ellipsoid (50%) plot and tagging scheme for **8**. (b) Packing diagram of **8**.

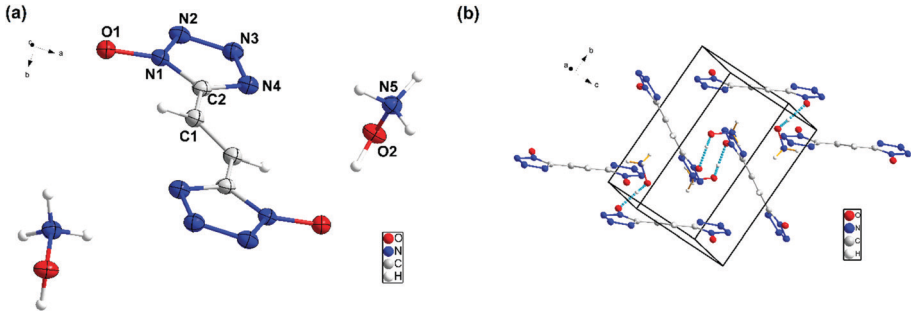

Fig. 6 (a) Thermal ellipsoid (50%) plot and tagging scheme for **9**. (b) Packing diagram of **9**.

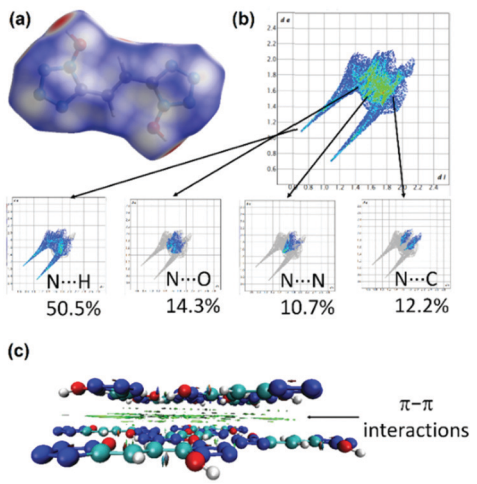

Fig. 7 (a and b) Hirshfeld surface graphs and 2D fingerprint plots of **6**. (c) Non-covalent interaction plots of gradient isosurfaces **6**.

5 °C min^{-1}. The decomposition temperatures (onset) for all the compounds occur between 226 (**6**) and 288 (**8**) °C (Table 1). Densities which were measured using a gas pycnometer at 25 °C, range between 1.47 (**7**) to 1.86 (**6**) g cm^{-3} (Table 1). To study the energetic properties of compounds **4–9**, the molar enthalpies of formation are calculated by using isodesmic reactions with the Gaussian 03 (revision D.01) suite of programs.

All the compounds have positive heats of formation (ΔH_f) which fall between 369.2 to 790.9 kJ mol^{-1}. Using the calculated HOFs and pycnometer densities, the detonation properties of compounds **4–9** are calculated with the EXPLO5 (version 6.06.02) code.[46] (Table 1). The detonation velocities (calculated) are between 7267 and 9017 m s^{-1}, and detonation pressures (calculated) range from 17.6 to 32.6 GPa, respectively. The detonation velocity (9017 m s^{-1}) of compound **6** is superior to RDX (8795 m s^{-1}). For comparison, we have also calculated the detonation properties of compounds **4–9** using the earlier EXPLO5 (version 6.01) code. The results are given in the ESI† (Table S1). The impact sensitivity and FS for compounds **4–9** are determined by using BAM standard methods. In comparison to RDX, compound **6** is less sensitive. In addition, the thermal stability and sensitivity properties of compound **6** are also found to be superior to compounds IV and V (Fig. 1 and Table 1).

Conclusion

In summary, the facile syntheses of ethane and ethene-linked bistetrazole derivatives were achieved. It was found that the incorporation of the ethene-link between tetrazoles leads to the planar structure and improved density. The density of the compound **5** (1.72 g cm^{-3}) was found to be significantly higher than compound **4** (1.50 g cm^{-3}), due to its planer structure. The density was further improved by synthesizing

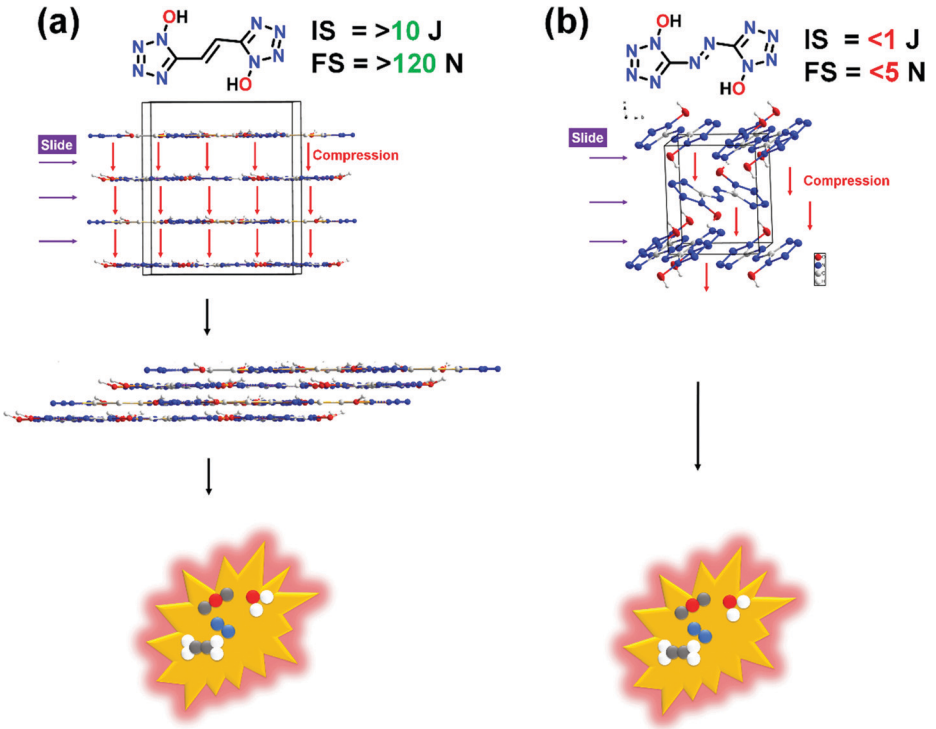

Fig. 8 Comparison of sensitivity properties of compound **6** with (*E*)-5,5′-(diazene-1,2-diyl)bis(1*H*-tetrazol-1-ol) (V).

Table 1 Energetic properties of compounds **4–9**

	T_d[a] (°C)	ρ[b] (g cm^{-3})	ΔH_f[d] (kJ mol^{-1})/kJ g^{-1}	P[e] (GPa)	D_v[f] (m s^{-1})	IS[g] (J)	FS[h] (N)
4	253	1.50	584.2/3.52	17.6	7267	>40	>360
5	275	1.72	790.9/4.82	24.6	8229	>20	>240
6	226	1.86/1.91[c]	776.9/3.96	32.6	9017	>10	>120
7	255	1.47/1.51[c]	369.2/1.59	20.1	7771	>40	>360
8	288	1.56/1.59[c]	597.7/2.60	23.6	8183	>40	>360
9	230	1.63/1.69[c]	553.3/2.11	26.8	8462	>40	>360
IV[i]	120	1.71	390.1	31.2	8711	1	<5
V[i]	170	1.90	883.2	42.4	9548	<1	<5
TNT[j]	295	1.65	−59.4/−0.26	19.4	6824	15	>353
RDX[k]	204	1.80	92.6/0.42	34.9	8795	7.5	120

[a] Temperature of decomposition (onset). [b] Density – gas pycnometer at 298 K. [c] Crystal density at 100 K. [d] Calculated molar enthalpy of formation. [e] Calculated detonation pressure. [f] Calculated detonation velocity. [g] Impact sensitivity (IS). [h] Friction sensitivity (FS). [i] Ref. 47. [j] Ref. 48. [k] Ref. 49. All compounds were obtained as anhydrous powders to determine the properties in Table 1.

the bis(1*H*-tetrazol-1-ol) derivatives. Compound **6** {(*E*)-5,5′-(ethene-1,2-diyl)bis(1*H*-tetrazol-1-ol)} exhibits a surprisingly high density of 1.91 g cm^{-3} at 100 K (1.86 g cm^{-3} at 298 K). The crystal structure of compound **6** gave more insight into the thermal stability and the sensitivity to external stimuli. The detonation properties of the compounds **4–9** were calculated using EXPLO5 (version 6.06.02). It was shown that the planar bis(1*H*-tetrazol-1-ol) derivatives **6** and **9** have good detonation performances, especially **6** exibits a detonation velocity of 9017 m s^{-1}, which is considerably superior to those of RDX (8795 m s^{-1}). Its decomposition temperature (226 °C), density (1.86 g cm^{-3}), and sensitivity to external stimuli (IS = >10 J and FS = >120 N) are also superior to those of RDX. Overall, the introduction of the planar ethene link between the bistetrazole and bis(1*H*-tetrazol-1-ol) derivatives improves the density of the compounds. The results of this research provide new insights for the further development of planer links for the synthesis of new high-energy-density materials.

Author contributions

J. S. investigation, methodology, and manuscript writing. R. J. S. X-ray data collection and solved the structures. J. S. and J. M. S. conceptualization, manuscript writing – review and editing, supervision.

Conflicts of interest

There are no conflicts to declare.

Acknowledgements

The diffractometer (Rigaku Synergy S) for SC-XRD was purchased with support from the National Science Foundation (MRI program) under grant no. 1919565. We are grateful to the Fluorine-19 fund.

References

1 T. M. Klapötke, *High Energy Density Materials*, Springer, Berlin, 2012.

2 J. P. Agrawal, *High Energy Materials*, Wiley, 2010.
3 D. Kumar and A. J. Elias, *Resonance*, 2019, **24**, 1253–1271.
4 T. M. Klapötke, M. Kofen and J. Stierstorfer, *Dalton Trans.*, 2021, **50**, 13656–13660.
5 M. S. Gruhne, T. Lenz, M. Rösch, M. Lommel, M. H. H. Wurzenberger, T. M. Klapötke and J. Stierstorfer, *Dalton Trans.*, 2021, **50**, 10811–10825.
6 L. Zeisel, N. Szimhardt, M. H. H. Wurzenberger, T. M. Klapötke and J. Stierstorfer, *New J. Chem.*, 2019, **43**, 609–616.
7 B. Wang, X. Qi, W. Zhang, K. Wang, W. Li and Q. Zhang, *J. Mater. Chem.*, 2017, **5**, 20867–20873.
8 Y. F. Gao, L. Zhang, L. He, Y. Zhao, N. Tang, W. L. Yuan and G. H. Tao, *RSC Adv.*, 2015, **5**, 54527–54534.
9 Y. Tang, H. Gao, D. A. Parrish and J. M. Shreeve, *Chem. – Eur. J.*, 2015, **21**, 11401–11407.
10 D. Kumar, G. H. Imler, D. A. Parrish and J. M. Shreeve, *New J. Chem.*, 2017, **41**, 4040–4047.
11 L. Türker, *Def. Technol.*, 2016, **12**, 1–15.
12 A. K. Chinnam, Q. Yu, G. H. Imler, D. A. Parrish and J. M. Shreeve, *Dalton Trans.*, 2020, **49**, 11498–11503.
13 J. Ma, A. K. Chinnam, G. Cheng, H. Yang, J. Zhang and J. M. Shreeve, *Angew. Chem., Int. Ed.*, 2021, **60**, 5497–5504.
14 T. Yan, G. Cheng and H. Yang, *ChemPlusChem*, 2019, **84**, 1567–1577.
15 J. Tang, H. Yang, Y. Cui and G. Cheng, *Mater. Chem. Front.*, 2021, **5**, 7108–7118.
16 J. Singh, R. J. Staples, J. P. Hooper and J. M. Shreeve, *Chem. Eng. J.*, 2021, **431**, 133282.
17 Y. Qu and S. P. Babailov, *J. Mater. Chem. A*, 2018, **6**, 1915–1940.
18 P. He, H. Mei, J. Yang and J. Zhang, *New J. Chem.*, 2019, **43**, 4235–4241.
19 V. A. Strunin and L. I. Nikolaeva, *Combust., Explos. Shock Waves*, 2013, **49**, 53–63.
20 A. E. D. M. van der Heijden and R. H. B. Bouma, *Cryst. Growth Des.*, 2004, **4**, 999–1007.
21 D. Chakraborty, R. P. Muller, S. Dasgupta and W. A. Goddard, *J. Phys. Chem. A*, 2000, **104**, 2261–2272.
22 J. Yang, G. Wang, X. Gong, J. Zhang and Y. A. Wang, *ACS Omega*, 2018, **3**, 9739–9745.
23 M. Reichel, D. Dosch, T. Klapötke and K. Karaghiosoff, *J. Am. Chem. Soc.*, 2019, **141**, 19911–19916.
24 Q. Lang, Q. Wang, Q. Lin, Y. Xu and M. Lu, *New J. Chem.*, 2021, **45**, 20542–20546.
25 W. Zhang, L. Bao, T. Fei, P. Lv, C. Sun and S. Pang, *CrystEngComm*, 2021, **23**, 8099–8103.
26 Q. Zhang, C. Zhao, X. Zhang, C. He and S. Pang, *New J. Chem.*, 2022, **46**, 1489–1493.
27 A. K. Yadav, V. D. Ghule and S. Dharavath, *Mater. Chem. Front.*, 2021, **5**, 8352–8360.
28 M. Göbel, K. Karaghiosoff, T. M. Klapötke, D. G. Piercey and J. Stierstorfer, *J. Am. Chem. Soc.*, 2010, **132**, 17216–17226.
29 J. Zhang, B. Jin, R. Peng, C. Niu, L. Xiao, Z. Guo and Q. Zhang, *Dalton Trans.*, 2019, **48**, 11848–11854.
30 X. Xu, D. Chen, H. Li, M. Yan, Y. Xiong, H. Zhao and R. Xu, *RSC Adv.*, 2020, **10**, 11939–11944.
31 C. Zhao, Y. Chi, Y. Xiong, Q. Yu, X. Wang, G. Fan and K. Yu, *Phys. Chem. Chem. Phys.*, 2019, **21**, 15215–15221.
32 Y. Cheng, X. Chen, N. Yang, Y. Zhang, H. Ma and Z. Guo, *CrystEngComm*, 2021, **23**, 1953–1960.
33 A. E. Sifain, L. F. Tadesse, J. A. Bjorgaard, D. E. Chavez, O. V. Prezhdo, R. J. Scharff and S. Tretiak, *J. Chem. Phys.*, 2017, **146**, 114308.
34 X. Yang, X. Lin, L. Yang and T. Zhang, *Chem. Commun.*, 2018, **54**, 10296–10299.
35 D. E. Chavez, D. A. Parrish, L. Mitchell and G. H. Imler, *Angew. Chem., Int. Ed.*, 2017, **56**, 3575–3578.
36 P. Yin, C. He and J. M. Shreeve, *J. Mater. Chem. A*, 2016, **4**, 1514–1519.
37 L. Hu, P. Yin, G. Zhao, C. He, G. H. Imler, D. A. Parrish, H. Gao and J. M. Shreeve, *J. Am. Chem. Soc.*, 2018, **140**, 15001–15007.
38 Y. Tang, W. Huang, G. H. Imler, D. A. Parrish and J. M. Shreeve, *J. Am. Chem. Soc.*, 2020, **142**, 7153–7160.
39 Z. Yin, Y. Dong, Z. Zeng, W. Huang and Y. Tang, *New J. Chem.*, 2021, **45**, 11752–11757.
40 Z. Yin, W. Huang, Z. Zeng, Y. Liu and Y. Tang, *Cryst. Growth Des.*, 2022, **22**, 1867–1873.
41 M. A. Spackman and J. J. McKinnon, Fingerprinting Intermolecular Interactions in Molecular crystals, *CrystEngComm*, 2002, **4**, 378–392.
42 M. A. Spackman and D. Jayatilaka, Hirshfeld surface analysis, *CrystEngComm*, 2009, **11**, 19–32.
43 T. Lu and F. Chen, Multiwfn: A multifunctional wavefunction analyzer, *J. Comput. Chem.*, 2012, **33**, 580–592.
44 E. R. Johnson, S. Keinan, P. Mori-Sánchez, J. Contreras-García, A. J. Cohen and W. Yang, Revealing Noncovalent Interactions, *J. Am. Chem. Soc.*, 2010, **132**, 6498–6506.
45 W. Humphrey, A. Dalke and K. Schulten, VMD: Visual Molecular Dynamics, *J. Mol. Graphics*, 1996, **14**, 33–38.
46 M. Sućeska, *EXPLO5 6.01*, Brodarski Institute, Zagreb, Croatia, 2013.
47 D. Fischer, T. M. Klapötke, D. G. Piercey and J. Stierstorfer, *Chem. – Eur. J.*, 2013, **19**, 4602–4613.
48 R. Mayer, J. Köhler and A. Homburg, *Explosives*, Wiley VCH, Weinheim, 6th edn, 2007.
49 Y. Tang, C. He, L. A. Mitchell, D. A. Parrish and J. M. Shreeve, C–N Bonded Energetic Biheterocyclic Compounds with Good Detonation Performance and High Thermal Stability, *J. Mater. Chem. A*, 2016, **4**, 3879–3885.